



Fate of arsenic-bearing phases during the suspended transport in a gold mining district (Isle river Basin, France)

Cécile Grosbois, Alexandra Courtin-Nomade, Eric Robin, Hubert Bril,
Nobumichi Tamura, Jörg Schäfer, G. Blanc

► To cite this version:

Cécile Grosbois, Alexandra Courtin-Nomade, Eric Robin, Hubert Bril, Nobumichi Tamura, et al.. Fate of arsenic-bearing phases during the suspended transport in a gold mining district (Isle river Basin, France). *Science of the Total Environment*, 2011, 409 (23), pp.4986-4999. 10.1016/j.scitotenv.2011.07.045 . insu-00624624

HAL Id: insu-00624624

<https://insu.hal.science/insu-00624624>

Submitted on 10 Oct 2011

HAL is a multi-disciplinary open access archive for the deposit and dissemination of scientific research documents, whether they are published or not. The documents may come from teaching and research institutions in France or abroad, or from public or private research centers.

L'archive ouverte pluridisciplinaire **HAL**, est destinée au dépôt et à la diffusion de documents scientifiques de niveau recherche, publiés ou non, émanant des établissements d'enseignement et de recherche français ou étrangers, des laboratoires publics ou privés.

Fate of arsenic-bearing phases during the suspended transport in a gold mining district (Isle river Basin, France)

C. Grosbois^a, Courtin-Nomade^b, E. Robin^c, H. Bril^b, N. Tamura^d, J. Schäfer^e, G. Blanc^e

^a Université François Rabelais de Tours, UMR 6113 CNRS ISTO, Université d'Orléans, Parc de Grandmont, 37200 Tours, France

^b Université de Limoges, Groupement de Recherche Eau Sol Environnement (GRESE), EA 4330, Avenue Thomas, 87000 Limoges cedex, France

^c Université d'Orsay, LSCE, UMR CEA/CNRS 1572, Av. de la Terrasse, 91198 Gif-sur-Yvette cedex, France

^d Advanced Light Source, Lawrence Berkeley National Laboratory, Berkeley, California 94720, USA

^e Université de Bordeaux, UMR 5805 CNRS EPOC, Av. des Facultés, 33405 Talence cedex, France

Abstract

Arsenic-rich ($\sim 140\text{--}1520 \text{ mg.kg}^{-1}$) suspended particulate matter (SPM) was collected daily with an automatic sampler in the Upper Isle River (France) draining a former gold mining district in order to better understand the fate of arsenic during the suspended transport (particles smaller than $50 \mu\text{m}$). Various techniques at a micrometric scale (EPMA, quantitative SEM-EDS with an automated particle counting including classification system and μ XRD) were used to directly characterize As-bearing phases. The most frequent ones were aggregates of fine clay particles. Their mineralogy varied with particle sources involved. These aggregates were formed by chlorite–phlogopite–kaolinite assemblages during the high flow and chlorite–illite–montmorillonite during the low flow. Among all the observed As-carriers in SPM, these clay assemblages were the least As-rich (0.10 up to 1.58 wt.% As) and their median As concentrations suggested that they were less concentrated during the high flow than during the low flow. Iron oxyhydroxides were evidenced by μ XRD in these clay aggregates, either as micro- to nano-sized particles and/or as coating.

(Mn, Fe)oxyhydroxides were also present as discrete particles. Manganese oxides (0.14–1.26 wt.% As) transport significantly more arsenic during the low flow than during the high flow (0.16–0.79 wt.% As). The occurrence of Fe oxyhydroxide particles appeared more complex. During the low flow, observations on banks and in wetlands of freshly precipitated Fe hydroxides (ferrihydrite-type) presented the highest As concentrations (up to 6.5 wt.% As) but they were barely detected in SPM at a microscale. During the high flow, As-rich Fe-oxyhydroxides (0.10–2.80 wt.% As) were more frequent, reflecting mechanical erosion and transport when the surface water level increased.

Arsenic transfers from SPM to corresponding aqueous fraction mostly depend on As-carrier stability. This study shows the temporal occurrence of each type of As-bearing phases in SPM, their As concentrations at a particle scale and abundance according to hydrological periods.

1. Introduction

During fluvial transport, trace elements (TE) are mostly bound to the fine solid fractions (silt/clay fractions) relative to their large specific surface areas which facilitate sorption, coating and/or complexation processes ([Gibbs, 1977] and [Horowitz, 1991]). Thus, a major concern of administrative management of river basins and environment survey agencies was potentially toxic sediment-associated TE dispersal during solid transport throughout a river basin as they were directly available for food-filtering organisms ([Paquin and Di, 2003], [Croteau et al., 2005] and [Wang and Fisher, 2009]). Specific attention was drawn to river systems affected by industrial and mining activities when high levels of certain TE were found in river sediments and exceeded toxic levels for river flora and fauna. For the past decades, legislative guidelines for contaminant dispersal focussed on absolute concentrations of bulk sediment fractions. However, TE transfers towards surface waters mainly depend on the type of associations between TE and particles. The stability of TE-carriers in the environment is then an important parameter to take into account in order to predict the long-term fate of contaminants such as TE.

The characterization of TE-carriers can be performed using selective and sequential extraction methods with different operationally defined fractions, derived from the protocol of Tessier et al. (1979). If this approach can be useful to quantify sediment-associated TE in the different fractions (e.g. [Kersten, 2002] and [Audry et al., 2006]), it can also be criticized for the use of non selective reactants ([Berrueta et al., 1995], [Gleyzes et al., 2002], [Kierczak et al., 2009] and [Anawar et al., 2010]) and the redistribution of some TE during the different operational steps ([Tipping et al., 1979], [Kheboian and Bauer, 1987] and [Belzile et al., 1989]). Therefore, direct observation techniques at a micrometric scale are necessary to assess the solid speciation of TE. Based on microanalysis procedures, the objective of this study was to characterize the nature of TE associations within the suspended material fraction. This study was carried out during the 2004–2005 hydrological year. To date, few studies have considered temporal variations of sediment-associated metal speciation ([Tessier et al., 1979], [Dawson and Macklin, 1998] and [Carter et al., 2006]) although hydrology and rainfall intensity variations in addition to seasonal variations of pH, redox potential, microbial activity and competing metal concentrations influence the stability of bearing-phases over a hydrological cycle. Therefore, this characterization of TE solid speciation was performed for different water flow conditions in order to assess the occurrence of TE-carriers during the solid transport.

2. Study area

2.1. Geological characteristics and mining past of the Upper Isle River basin

The Upper Isle River basin, being one of the 2 major tributaries of the Dordogne River system in the Gironde estuary watershed (SW France, Fig. 1), includes the former 2nd most gold productive district of France (Nicaud, 2001) with a basin surface of 432 km². The gold mining district is located on an Au-productive veins in granites, ortho- and para-gneiss where hydrothermal alteration, synchronous with ore deposition, resulted in a phengite + chlorite association, and then a chlorite + carbonate assemblage (Touray et al., 1989). The entire Au-mining district is located on an As-geochemical anomaly, with primary As-host minerals like arsenopyrites and arsenian pyrites in granitic and gneissic bedrock. The natural mean geochemical background in arsenic, determined in non-mining influenced areas, is ~ 120 mg/kg in soils (Chery and Gateau, 1998), ~ 70 mg/kg in bed sediments (Grosbois et al., 2007) and ~ 10 µg/L in the < 0.45 µm aqueous fraction (Grosbois et al., 2009). Therefore, in the solid fraction (bed sediments and soils), the most enriched trace-element is arsenic in

comparison to the regional geochemical background ([Grosbois et al., 2007] and [Bossy et al., 2010]).

This gold district has been intensively exploited from the early 1910s to 2000, the most important gold production period being between 1982 and 2000. Over 1 400 000 tons of mining wastes, including tailings, have been generated (Nicaud, 2001). During the studied hydrological year 2004–2005, some gallery outlets and mine tailing weathering effluents were still directly discharged into the Isle riverpath (as described previously by [Roussel et al., 2000] and [Bodénan et al., 2004]) and some contamination influence has been evidenced in the aqueous fraction (Grosbois et al., 2009). Nowadays, some remediation efforts are currently underway, including protection dams, groundwater aeration steps and ferric flocculation-based water treatment. The monitoring station of this study was located at the outlet of the former mining district (Fig. 1), collecting all the potential mining outputs, and draining only crystalline bedrock of the upstream basin i.e., located upstream from the areas of the Dordogne River basin covered by sedimentary bedrocks.

2.2. Climatic and hydrological characteristics

The climate of the studied area is mainly oceanic with some continental influence due to the higher altitudes of the eastern part of the Dordogne basin. The average of monthly cumulated rainfall (1971–2000) ranged from 52 mm in July to 85 mm in December with an average annual rainfall volume of 860 mm (www.meteo.fr). The studied period 2004–2005 was relatively dry as the basin only received 720 mm of rainwaters.

At the monitoring station, the mean annual water flow, calculated for the 1990–2004 hydrological years from the hydrology database of the Ministry of Ecology (www.hydro.eaufrance.fr), ranged between $82 \times 10^6 \text{ m}^3/\text{y}$ in 1991–1992 and $380 \times 10^6 \text{ m}^3/\text{y}$ in 1992–1993 with a median value of $190 \times 10^6 \text{ m}^3/\text{y}$. The studied period 2004–2005 was then a dry hydrological year ($106 \times 10^6 \text{ m}^3/\text{y}$) with a low flow period lasting about 7 months (low flow when discharge $< 5 \text{ m}^3/\text{s}$ from 04/09/09 to 04/12/16 and from 05/05/22 to 05/09/08; 213 days) which was much longer than the dry periods usually observed from July to October. During this low flow period, the daily discharge ranged from 1.4 to $4.2 \text{ m}^3/\text{s}$. During the high flow period (when discharge $\geq 5 \text{ m}^3/\text{s}$; 152 days from 04/12/17 to 05/05/21), the daily discharge increased up to $23 \text{ m}^3/\text{s}$. Winter floods were well identified as individual episodic with a rapid discharge increase, lasting less than 3 days, and a slower discharge decrease, lasting at least one week. Each flood event corresponded to a rain event $> 18 \text{ mm/day}$ (Grosbois et al., 2009).

The nature of impermeable but fractured crystalline bedrock, incised riverbank morphology and surrounding steep slopes indicate that the study area presents an unconfined and shallow adjoining aquifer plus additional small aquifers at higher altitude than the riverpath. Based on geochemical end-member identification and quantification in surface water chemical composition, groundwaters from the adjoining aquifer probably are the main supply to the Isle River surface waters during the low flow (Grosbois et al., 2009). During the high flow, contributions of rainwaters, runoff and hyporheic flow provide waters and dissolved TE to both aquifers and surface waters.

3. Analytical methods

3.1. Sample collection

An automatic sampling system (SIGMA 900) has been used to collect 8 sub-samples per day (one sample every 3 h) of 120 mL of waters cumulated in acid pre-cleaned 1-L polypropylene bottles. Every time bottles were replaced in the automatic sampler (every 20 to 24 days), 1 L of unfiltered river water was collected and stored in an acid cleaned sampling bottle and placed in the automatic sampling system during the following 24-day period. Another sample was also taken at the same moment and processed after arrival in the laboratory (within 2 h). Comparison of results obtained for these sample aliquots allowed checking potential sample alteration during up to 24 days of storage in the sampling device e.g., by potential sorption onto bottle walls and particle surfaces. Less than a 15% difference was observed in suspended matter concentrations and chemical concentrations of suspended materials.

Each daily sample was processed to determine SPM concentrations on pre-weighed 0.45 µm cellulose acetate filters. Suspended particulates were pressure-filtered through pre-weighed 0.45 µm Teflon filters (Millipore® LCR) and then air-dried. Series of filter blanks (ultrapure water; MilliQ®) were also done in the field in order to verify the absence of filter contamination and/or errors in the sampling protocol. For particulate bulk element concentrations, 102 samples, among 318 collected, were analyzed according to daily discharge variations, SPM concentrations and sample position in flood episode chronology. This represented on average one sample every 3 days. During the hydrological cycle, flood deposits when available and surface waters (5 L) were collected in order to get enough solid material for mineralogical determination.

3.2. Analytical methods

3.2.1. Physical characterization of the solid material

Grain-size distribution of the SPM fraction was measured using the particle size analyzer Hydro 2000S Mastersizer (Malvern) with dual-wavelength detection system (466 and 633 nm). About 1 g of air-dried SPM material was dispersed in 10 mL of deionized water plus 0.1% Na hexametaphosphate solution during 15 min ultrasonic treatment to ensure sample dispersion. Three replicates of 1 to 3 mL of the suspension sample were flushed onto the measurement cell in order to obtain 10% obscuration of the laser beam. Used refractive index was 1.45 (= silica). As the grain-size output ranged from 0.05 µm to 2 mm assuming spherical geometry of particles, only the median diameter d_{50} of particles was then used.

The bulk mineralogy of the SPM air-dried fraction was determined on unoriented sample powder tiles by X-ray diffraction (XRD) using a CuK α radiation (step size = 0.04° 2 θ ; counting time = 28 s/step, between 2.5° and 70°) on a Siemens D5000 diffractometer, equipped with a diffracted-beam graphite monochromator designed to minimize the fluorescence effect. The mineralogical phase determination was carried out with XPert HighScore version 2.0 software using the ICDD database.

3.2.2. Chemical characterization of suspended particles

Thin sections were prepared from flood deposits and from SPM air-dried material on Teflon filters. Suspended particulate material was included in epoxy resin, Teflon filter up-side down. Teflon filters were gently removed and then, particles were polished and carbon coated to be observed with a Philips XL-30 scanning electron microscope (SEM) using an

accelerating voltage of 20 kV coupled to an energy dispersive X-ray system (EDS) for element identification and mapping.

Two methods were then used to quantify major and trace element concentrations in As-bearing particles. One method classically used an electron X-ray microanalyzer Cameca SX50 (EPMA) at 15 kV with a 4 nA beam current on polished and carbon coated thin sections. Under these analytical conditions, the analyzed volume in the thin section was about $2 \mu\text{m}^3$.

Another method used a calibrated SEM (JSM 840) equipped with an EDS system from PGT and with an automated particle counting and classification (ACC) system developed by [Robin et al., 2003] and [Robin and Molina, 2006]. Several milligrams of material was well-ground in an agate mortar. Aliquots of about 200 μg were dispersed in alcohol using an ultrasonic apparatus and then filtered on a 0.5 μm Nuclepore® filter (surface of filtration 25 mm^2). The filters were then mounted on a carbon sample-holder and coated with carbon for SEM observations. In a first step, a numerical image is acquired from the backscattered electron beam with typical resolution and magnification of 1024×1024 pixels and $\times 1000$, respectively. The position and shape parameters of each detected particle are then determined and stored. A total of 50 images per sample randomly dispersed over the filter are thus acquired. In a second step, multi-element spectra are acquired for particles having minimum and maximum sizes of 0.5–5 μm using a high purity germanium detector and digital pulse processing. The probe current is set at 6 nA and 25 kV with a counting time of 50 s/particle allowing the counting of about 1000 particles in one night. Particles are then automatically sorted into 6 classes based on chemical criteria. These classes were experimentally tested and defined as Fe-rich oxides, (Fe, Mn)-rich oxides, silicates, Ca-rich particles, As-rich particles (see Annex I.1 for chemical criteria). In a third and last step, multi-element spectra of the classified particles are automatically compared to a series of pure reference spectra and X-ray absorption and fluorescence effects are corrected using ZAF program supplied by PGT. This enabled us to carry out quantitative analyses for O, Na, Mg, Al, Si, P, S, K, Ca, Ti, Cr, Mn, Fe, and As simultaneously. The precision is about 5% of the measured value for major elements and the sensitivity is 0.1 wt.%. Chemical composition of each particle was then validated according to its EDS-spectrum and molar ratios $O_{\text{meas}}/O_{\text{stoichio}}$ over 1, O_{meas} representing the amount of oxygen measured with the SEM/EDS-ACC system. Elemental concentrations $[X]_{\text{norm}}$ were normalized to stoichiometric totals (Tot_{stoichio} ; calculation in Annex I.2). In addition, the detection limit of As was experimentally estimated to 0.1 wt.% and the data presented here will be therefore for particles with As concentrations $\geq 0.1 \text{ wt.}\%$.

This second technique allowed counting a larger number of individual particles (about 1000 per sample) than strictly SEM observations and subsequent EPMA analyses. To be able to compare results acquired by the two analysis procedures, major and trace element concentrations, produced by EPMA, were also normalized to stoichiometric totals as $[X]_{\text{EPMA norm}}$ as follows:

$[X]_{\text{EPMA norm}} = [X]_{\text{measured by EPMA}} / Tot_{\text{stoichio}} 100$, where $[X]_{\text{EPMA norm}}$ represents the EPMA normalized concentration of the element X in the analyzed particle, $[X]_{\text{measured by EPMA}}$ the concentration of the element X analyzed by EPMA technique and Tot_{stoichio} the stoichiometric total calculated as for SEM/EDS-ACC system (Annex I.2).

Averages and ranges of normalized concentrations were compared for both analysis techniques in particles of one sample of suspended matter collected in December 2004 (Annex I.3). Except for Na and S, variations of major and trace element concentrations in the

different types of As-carriers were in the same range of magnitude, indicating the absence of any strong measurement/calculation bias. Therefore, results were presented according to the type of carriers instead of the type of analysis technique hereafter. For Na and S, minima obtained by EPMA were consistently one order of magnitude lower than for SEM/EDS-ACC analyses. This loss of Na and S during EPMA analyses may be related to element volatilization during an excess heating of analyzed particles.

3.2.3. Mineralogical characterization of suspended particles

Mineralogical characterization of suspended particles was performed by micro scanning X-ray diffraction (μ SXRD) at the ALS beamline 12.3.2 (Lawrence Berkeley National Lab, Ca, USA) (Kunz et al., 2009) with an analytical procedure defined in Courtin-Nomade et al. (2010) on the same polished thin sections than for SEM and EPMA analyses, after carbon coatings has been removed. Each analyzed area has been firstly mapped for Fe by micro-scanning-X-ray fluorescence (μ SXRF) on the same beamline and using similar configuration than for μ SXRD analyses. Micro-SXRD patterns were then collected using a monochromatic mode because of the small size of the analyzed particles. Thin sections were mounted onto an XYZ stage horizontally tilted at 6°, with an incident X-ray energy of 10 keV, a beam size of 2 μ m (H) \times 20 μ m (V) [beam footprint size on the sample of 20 μ m (H) \times 20 μ m (V) FWHM] and a Mar133 CCD detector (1 \times 1 k pixels binned mode). Acquisition times for micro X-ray patterns varied from 30 s up to 300 s according to the nature of the analyzed phase and its crystallinity in order to obtain significant intensity for each peak. Acquisition time for micro-XRD mineralogical maps varied from 6 to 8 h per map, depending on the size of the analyzed surface. Results were extracted using the software XMAS (Tamura et al., 2005) and a NIST corundum powder calibration material.

4. Results and discussion

4.1. Physical characteristics of suspended particles

Concentrations of SPM ranged from 2 to 25 mg/L during the low flow (discharge $< 5 \text{ m}^3/\text{s}$) and up to 135 mg/L during the high flow (Fig. 1). During this high flow period, a succession of clockwise and anti-clockwise SPM concentrations vs discharge hysteretic relationships was observed, each flood peak corresponding to a SPM concentration maximum. These SPM concentration variations represented an annual SPM flux of $\sim 2390 \text{ t/y}$ (calculated with daily discharge and measured daily SPM concentrations during the hydrological year September 2004-August 2005). This corresponded to a specific annual flux of $5.5 \text{ t/km}^2/\text{y}$ and was in the low range of specific fluxes of other sub-basins of the Gironde estuary basin (Masson et al., 2007).

Variations of SPM median grain size were in the same range during all the hydrological cycle. The largest length of particles, observed by SEM, was generally less than 60 μ m with a d_{50} of 15 μ m during the low flow and of 22 μ m during the high flow. Based on SEM observations, particles had round shapes in an organo-clay matrix or in particle agglomerates except for sheet particles which showed a more angular shape. Suspended particles were composed of various primary silicates and clay minerals according to the geology of the Upper Isle River Basin as it was previously reported for bed sediments (Grosbois et al., 2007). Present silicates, determined by XRD on bulk solid fraction, were quartz, feldspar-group minerals and chlorite-group minerals (Fig. 1). This main mineralogical assemblage appeared to be similar during the low and the high flow periods (Fig. 1). No specific arsenic-bearing mineral could be

directly identified with XRD technique on bulk material, probably due to a very small abundance (< 5% by weight) in respect to described analytical conditions. Thus, micrometric scale technique was carried out to characterize As-bearing phases.

4.2. Chemical and mineralogical variability of As-bearing particles at a micrometric scale

Arsenic-bearing phases in SPM were characterized using SEM and EPMA techniques in order to determine physical and chemical characteristics of each As-carrier type. They were also analyzed by automated SEM/EDS-ACC system in order to access the representativity of each As-carrier type with a large number of discrete analyzed particles. Temporal variations of As-carrier type occurrence were calculated with only SEM/EDS-ACC data to ensure consistency of results. It was calculated as the ratio between the number of one As-carrier type and the total of analyzed particles with detected As during one hydrological period.

The major As-carriers, according to their increasing occurrence, were Mn oxyhydroxides, Fe oxyhydroxides and aluminosilicate aggregates. Two other less frequent carrier types were detected by only the SEM/EDS-ACC system: arsenates and Mn-rich hydrous silicates. Relative to their high density, no relict sulfides were transported in suspension materials although they were the most As-concentrated carriers in bed sediments in this studied basin (Grosbois et al., 2007). All these different types of As-bearing phases were described subsequently according to hydrological periods.

4.2.1. Arsenic-bearing phases during the high flow

During the high flow, the present As-bearing phases were clay aggregates, Fe oxyhydroxides and Mn oxides plus Mn-rich hydrous silicates from the most to the least frequent As-carriers respectively.

4.3. As-rich aluminosilicate aggregates

This type of As-bearing phases looked like small (no longer than 20 µm) and loose aggregates of fine discrete grains in an organic-clay matrix (Fig. 2 and Fig. 6). According to X-Ray diffractograms of the bulk fraction, clay minerals were dominated by chlorite, micas (muscovite-type) and illite (Fig. 1) along the studied annual cycle. These phases contained Si and Al as major elements with concentrations ranging from 12.4 to 45.1 wt.% Si and from 7.9 to 29.6 wt.% Al (Table 1a).

According to Fe concentrations, 2 groups could be distinguished in these aggregates: (i) clays with Fe concentrations < 10 wt.%, Si + Al concentrations being at least twice those of Fe concentrations and (ii) Fe-rich aggregates with Fe concentrations higher than 8 wt.% and in the same range of Si and Al contents. In order to differentiate the mineralogy of these 2 groups, we used ternary diagrams based on elemental composition and the clay mineral classification of Velde (1985; Fig. 3). Elemental compositions presented a large dispersion between 3 end-members ($\text{Si}/4$; $\text{Na} + \text{K} + 2\text{Ca}$; $(\text{Mg} + \text{Mn} + \text{Fe})/3$). Chemical composition, as determined by EPMA, of natural and well-identified clay minerals by Deer et al. (1967) was also added for references.

The 1st group “clays” represented 57% of all the analyzed As-rich particles by SEM/EDS-ACC system during the high flow. Their mineralogy was an assemblage of muscovite/illite, phlogopite, montmorillonite and kaolinite when compared with the composition of clay

minerals determined by Deer et al. (1967). Major cations of these clays were K, up to 10.5 wt.% K, like in illite and muscovite structure (Deer et al., 1967). K/Al molar ratios of these aggregates ranged from 0.02 to 0.75 which was close to the ones of illite and muscovite (respectively 0.07–1.7 and 0.2–0.4; Deer et al., 1967). They also contained some magnesium, up to 6.1 wt.% Mg. Among all the As-bearing phases identified, this group of clays was poorly As-concentrated with concentrations ranging from 0.1 up to 1.6 wt.% As (Table 1a).

The 2nd group was defined as “Fe-rich aluminosilicate aggregates”. They were also highly representative of As-rich bearing phases with 32% of all the analyzed particles over the high flow. Their mineralogy varied from chlorite to phlogopite (Fig. 3). Potassium concentrations were lower than for the previous group (not more than 4.4 wt.% K) and the major cation was Mg, up to 11.5 wt.% Mg (Table 1a) in the same range as phlogopite (ranging from 9.4 to 17.2 wt.%; Deer et al., 1967). This group had As concentrations maxima in the same range as the previous type of clays, from 0.1 to 1.4 wt.% (Table 1a). For both groups, these identified mineralogical assemblages in SPM were consistent with the degree of laterisation of the studied area during the late Paleozoic era and hydrothermal alteration of quartz veins ([Bouchot et al., 1989], [Touray et al., 1989] and [Piantone et al., 1994]) and consecutive weathering sequence in the Upper Isle Basin (Proust et al., 1986).

However, in both types of aggregates, As concentrations were significantly and positively correlated to the ones of Fe and P ($r = 0.43$ and $r = 0.44$ respectively; $p < 0.005$; $n = 194$) but did not show any significant correlation neither with Si nor Al concentrations. According to SEM observations, these aggregates included grains of different mineralogy (Fig. 2, Fig. 4 and Fig. 6) as previously observed by Hochella et al. (2005), who reported the presence of nanocrystalline sulfides and Mn oxides in various clays of floodplain sediments. Thus, SEM and EPMA analyzes may only give an averaged chemical composition of several grains due to their very small size with respect to the beam size and overlapping of discrete isolated grains in the aggregates. This could explain why chemical composition did not match clearly with any ideal structural formula of clays. Some high Fe contents (up to 35.5 wt.% Fe during the low flow and up to 25.3 wt.% Fe during the high flow) in several observed aggregates were higher than for Fe-rich clays like illite or muscovite (from 1.1 up to 5.5 wt.% Fe; Deer et al., 1967) and chlorite compositions (from 10.9 up to 33.9 wt.% Fe, Deer et al., 1967). Such high Fe contents could be related to the presence of (i) Fe-oxyhydroxide coatings on clay particles or/and (ii) micrograins of Fe oxyhydroxides included within the aggregates as suggested from (Fe, As) significant relationships. Therefore, micro X-ray diffraction was performed to better discriminate the mineralogical assemblage of these aggregates. This approach evidenced that some goethite was present within the studied clay aggregates. The μ XRD mineralogical maps clearly showed the distribution of several Fe-host phases in the same aggregate (Fig. 4) like goethite, chlorite and muscovite at their main intensity XRD peak (respectively, 4.18 Å, 7.07 Å and 9.9 Å). Therefore, the defined group as Fe-rich aluminosilicate aggregates finally corresponded to Fe-rich clays like chlorites and smectite group (nontronite end-member) associated to Fe oxyhydroxides either as micro- to probably nano-sized grains and/or as coatings on clays. In order to distinguish between these 2 potential physical aspects of Fe oxyhydroxides, high resolution images could have been done with a transmission electron microscope but the probability to insert a clay aggregate, enriched in iron and bearing arsenic in a TEM mesh grid was too low.

4.4. As-rich Fe oxyhydroxides

As-rich Fe oxyhydroxides appeared as isolated particles in the organo-silicated matrix, presenting either a very compact and homogeneous aspect or a fluffy one. Their size usually ranged from 10 to 60 µm for the longest length (Fig. 4). They represented 7% of all the observed As-rich particles by SEM/EDS-ACC system during the high flow.

This type of As-carrier was determined as Fe oxyhydroxides when Fe was the only major element, Fe normalized concentrations ranging from 26.7 to 55.7 wt.% Fe (Table 1a) when the other elements were lower than 15 wt.%. Elemental totals ranged from 55 to 65 wt.%. The lowest totals highlighted the hydrated/hydroxylated characteristics of these compounds and µXRD patterns of Fe oxyhydroxides mainly showed the presence of goethite.

Some of these particles were very homogeneous chemically. Some other particles looked more like mineral associations (Fig. 4). In fact, elevated Ca concentrations, up to 8.5 wt.% Ca, were reported in these As-rich oxyhydroxides, which was already observed by [Patkunc et al., 2004] and [Drahota et al., 2009]. They also contained significant amounts of Mn (up to 4.9 wt.% Mn), very well localized in the studied particles (Fig. 5). Trace elements, contained in these particles, were some CuO, PbO and ZnO (< 7000 mg/kg) when detected but the most abundant TE was As with concentrations up to 2.5 wt.% As. These carriers also had P (up to 3.1 wt.%) as P usually competes with As when sorbed on Fe oxyhydroxides ([Dixit and Hering, 2003] and [Gordeev et al., 2004]). Amounts of Si (up to 15.3 wt.%) and of Al (up to 12.0 wt.%) were detected although no significant correlation between all these elements was outlined. As the presence of goethite in clay aggregates was related to the highest Fe amounts by EPMA, the presence of Si and Al in these grains could come from clay fine grains intimately associated with Fe oxyhydroxides as previously described for As-rich aluminosilicate aggregates. In Fig. 6, a diffractogram was obtained by µXRD in the most concentrated Fe area containing As (point #13 with 18.3 wt.% Fe and 0.1 wt.% As). This highlights the presence of a particle or a coating of goethite associated here with Fe-rich clays like chlorite and muscovite.

4.5. As-rich Mn oxyhydroxides and Mn hydrous silicates

Mn-rich particles were identified as Mn oxyhydroxides and Mn-rich hydrous silicates according to Mn, Si and Al concentrations. They all were very rare during this hydrological period representing less than 5% of the total observed As-rich particles.

Manganese oxyhydroxides with detectable As were not as numerous as Fe oxyhydroxides (9 and 31 particles, respectively during this hydrological period). In this type of As-carriers, Mn levels ranged from 30.8 up to 42.8 wt.% Mn (Table 1a). They were sometimes present as discrete and small particles (< 10 µm for the longest length) but most of the time they were included in larger particles of Fe oxyhydroxides and/or in aluminosilicate aggregates (point #3 in Fig. 2 and point #10 in Fig. 5). The mineralogical name of these Mn oxyhydroxides was hardly evidenced by µXRD technique due to (i) the low intensity of XRD peaks of Mn species and (ii) the overlapping of XRD peaks with clay minerals. When detected, As concentrations in these particles ranged from 0.16 to 0.79 wt.% As. No clear correlation between Mn and As amounts occurred and elemental EDS maps showed an homogeneous spatial distribution of arsenic within this type of particles, i.e. no As concentrated areas.

In Mn-rich hydrous silicates, manganese was less concentrated than in Mn oxyhydroxides, ranging from 12.0 to 26.9 wt.% Mn. The presence of Si, Al and Fe was very well marked as their respective concentrations were in the same range (Table 1a). In these cases, the lowest Mn concentrations corresponded to the highest (Al, Si) amounts. Although we did not observe any significant statistical correlation between Mn and Fe concentrations in this type of carrier, significant negative correlations between Mn and Si or Mn and Al occurred ($r = 0.67$ and $r = 0.68$ respectively; $p < 0.005$; $n = 46$; Fig. 2). The major cations were Ca and Na during this high flow period. This type of As-carriers contained up to 0.71 wt.% As when detected (Table 1a). The mineralogical classification of Mn-rich hydrous silicates can be complex and chemical compositions frequently are different from the ideal structural formula. For example, the ganophyllite-like minerals are complex modulated layer silicates (Hughes et al., 2003) with structural formulae like $(K, Ca, Na)_xMn_6(Si_9Al)O_4(OH)_4.nH_2O$ (ganophyllite for the K end-member, tamaite for Ca end-member and eggletonite for Na end-member; [Applin, 1958] and [Eman et al., 2009]). They present various Mn contents ranging from 27.4 wt.% in the Na end-member ([Peacor et al., 1984] and [Eggerton and Guggenheim, 1986]) down to 21.8 wt.% in the K end-member. Their Si contents can range from 16.7 wt.% in the K end-member to 19.2 wt.% in the Na end-member. Their Al contents increase with decreasing Si contents, from 1.68 wt.% in the Na end-member up to 5.88 wt.% in the K end-member. This chemical variability corresponds to the range of (Si, Al, Mn) contents in Mn hydrous silicates of the Upper Isle River. Furthermore, in our samples, μ XRD evidenced kellyite $[(Mn, Mg, Al)_3(Si, Al)_2O_5(OH)_4]$ and hisingerite-neotocite serie $[(Fe, Mn)SiO_3, H_2O]$ (Fig. 5). Kellyite belongs to the (Mn-Al) serpentine group (Bergaya et al., 2006) and can contain from 25.4 up to 30.0 wt.% Mn with a Si/Al molar ratio ranging from 0.52 to 1.51 (Peacor et al., 1984). Neotocite, the Mn end-member, is a poorly ordered Mn hydrous silicate, occurring with different stages of silicate mineral alteration in various geological environments ([Eggerton and Guggenheim, 1986] and [Shayan, 1984]). Thus, As-bearing phases containing Mn in the Upper Isle River SPM could correspond to a mixture of different Mn-rich hydrous silicates.

4.5.1. Arsenic-bearing phases during the low flow

During the low flow, As-bearing phases were mostly the same as during the high flow but they presented different ranges of compositions and various occurrences. In addition, a few grains ($n = 7$), detected with the SEM/EDS-ACC system, could correspond to Fe-rich arsenate minerals. Therefore, As-bearing phases were presented from the most to the least frequent during this hydrological period.

4.6. As-rich aluminosilicate assemblages

The same 2 groups have been observed during the low flow than during the high flow and they were still the most abundant. The 1st group, called clay aggregates, represented 75% of all the analyzed As-rich particles during the low flow (57% during the high flow). The 2nd group, corresponding to Fe-rich clay and Fe oxyhydroxide assemblages, was less present than during the high flow with 18% (32% during the high flow). The main mineralogical differences between the 2 hydrological periods were (i) the kaolinite end-member seemed to be absent from the “clay” group as no kaolinite grains were directly observed during the low flow. This may be linked to a smaller spectrum of mobilized particle sources during the low flow when erosion and bedrock runoff is low; (ii) the mineralogical composition of Fe-rich aluminosilicate aggregates looked consistently present but less dispersed during the low flow than during the high flow (Fig. 3).

Median As concentrations were higher during the low flow than during the high flow in both groups, although the range of As concentrations was similar (Table 1b). Median As concentrations were about 0.21 ± 0.55 wt.% ($n = 142$) in the 1st group and about 0.39 ± 0.38 wt.% ($n = 52$) in the 2nd group. In sub-neutral pH and oxic conditions like the Upper Isle River basin, montmorillonite, chlorite and illite have much greater sorption capacities for dissolved As(V) than kaolinite ([Manning and Goldberg, 1996] and [Manning and Goldberg, 1997]). Hence, clay aggregates containing kaolinite contained less arsenic, especially during the high flow. Few studies reported on the role of As sorption on clay minerals for natural attenuation in the environment and in mining/industrial site remediation ([Lin and Puls, 2000], [Manning and Goldberg, 1996] and [Manning and Goldberg, 1997]). They all showed the weak affinity of these materials for As when compared to Fe oxyhydroxides which was consistent with lower As concentrations in these 2 types of aggregates compared to particles of Fe oxyhydroxides in Isle River SPM.

4.7. As-rich Fe oxyhydroxides

Isolated particles of Fe oxyhydroxides were almost not detected during the low flow with SEM/EDS-ACC technique (2% of all the analyzed As-rich particles) but EPMA technique allowed specifically to observe additional particles of Fe oxyhydroxides ($n = 45$). They showed higher Fe concentrations during this hydrological period than during the high flow when median Fe values were 55 ± 8 wt.% Fe and 33 ± 7 wt.% Fe respectively. On the opposite, they were less concentrated in As (median 0.31 ± 0.57 wt.%) than during the high flow (median 0.68 ± 0.60 wt.%). In addition, totals of these analyzed Fe oxyhydroxides were higher during the low flow than during the high flow (Table 1b) and they could be related to ageing processes leading to the presence of better organized Fe oxyhydroxides during this low flow period. As detailed by Cornell and Schwertmann (1996), Fe hydroxides can evolve into Fe oxides when dehydrated and deshydroxylated. These mechanisms tend to increase Fe concentrations and result in a better structural organisation. Accordingly, dehydrated Fe oxides can trap arsenic, being more strongly bound to the more stable phases (Pedersen et al., 2006) but Gautier et al. (2006) also showed that arsenic could be released as the number of available sorption sites decreased, which could correspond to observations made in the Isle River SPM during the low flow.

In addition, in the Isle River basin during the low flow period, authigenic Fe(III) hydroxides (ferrihydrite-type, Gautier et al., 2006) were observed on banks and surrounding wetlands (Grosbois et al., 2007) and in mining sites ([Roussel et al., 1998] and Courtin-Nomade, 2001) when sub-anoxic waters from adjacent aquifer contributed to surface waters (Grosbois et al., 2009). They contained up to 9.1 wt.% As with molar Fe/As ratios around 4 (Grosbois et al., 2007). However, they were barely quantified by SEM/EDS-ACC technique in low flow SPM. Such Fe hydroxides may be rarely transported in the SPM fraction during this period due to either (i) their high solubility (Cancès et al., 2008), and/or to (ii) the too low stream water level and to the very low rate of mechanical erosion to mobilize them during the low flow period.

4.8. Mn-rich particles

The least frequent As-carrier type was Mn-rich particles, either as Mn-rich hydrous silicates or as Mn oxides during the low flow, lower than 3% like during the high flow. Manganese-rich hydrous silicates had similar As contents during both hydrological periods with As median concentrations of 0.42 ± 0.22 wt.% As during the low flow (0.33 ± 0.15 wt.% As

during the high flow). Any temporal variations could have been described with such low number of particles.

In Mn oxyhydroxides, Mn concentrations ranged from 34.6 wt.% up to 63.6 wt.% during the low flow. They globally contained more Mn and As during the low flow than during the high flow.

4.9. Arsenate minerals

Some particles presented the highest As contents, widely ranging from 14.6 wt.% up to 41.4 wt.% (Table 1b) and they could correspond to some arsenate minerals with a Fe/As molar lower than 1.5. These arsenate minerals were very rare and only detected with the SEM/EDS-ACC system in low flow SPM. They also contained sulphur, S concentrations ranging from 4.6 up to 11.7 wt.% S with molar As/S ratios ranging from 1.16 to 1.72. They presented some high concentrations in Si and Ca, i.e. up to 15.2 wt.% and 6.0 wt.%, respectively and they showed no measurable P, low Fe and Mn, with concentrations lower than 3.0 wt.% and 0.3 wt.%, respectively. Although Fe-arsenates (pharmacosiderite group, (Ba, Na, K)Fe₄(AsO₄)₃(OH)_{3.6}H₂O)) were commonly observed in weathered bedrock and in the corresponding saprolite of the Upper Isle River soil (Bossy et al., 2010), any of SPM arsenate minerals did not correspond to these Fe-arsenate chemical composition. Two of these grains could be Ca-arsenates with typical Ca/As molar ratios (1.25–4.0; Zhu et al., 2006) which could form with lime addition in fields and in small lakes to increase water pH.

These As-richest particles may be secondary formed when the environment was highly concentrated in dissolved arsenic (Drahota and Filippi, 2009). Studied surface waters did not appear oversaturated for any type of arsenates during the studied period (dissolved As ranging from 7 to 35 µg/L; Grosbois et al., 2009). Therefore, they probably formed upstream in mining sites, in weathered bedrock and corresponding alterites and/or wetlands as described in several studies ([Juillot et al., 1999] , [Drahota and Filippi, 2009] and [Bossy et al., 2010]) but they were barely transported by SPM.

4.10. Potential transfer of arsenic during the solid transport towards the dissolved fraction

Suspended particulate material of the Upper Isle River presented a similar mineralogical assemblage during the solid transport (except arsenate minerals detected only during the low flow) although the proportions of each As-carrier varied (Table 1). During the high flow, the most abundant As-carriers were clay aggregates (muscovite/illite, kaolinite, montmorillonite) and Fe-rich clays (chlorite, phlogopite, nontronite) associated to Fe oxyhydroxides, either as fine discrete grains or/and coatings. A kaolinite end-member was very well-marked in high flow SPM and was related to additional particle sources during this hydrological period. Iron oxyhydroxides and Mn-rich particles (Mn oxides and Mn-rich hydrous silicates) were less present in the SPM assemblage but they had much higher As concentrations than clay aggregates. This represented an As flux of 900 kg throughout this period (about 800 kg of arsenic transported by clays and Fe-rich clays, 60 kg by Fe oxyhydroxides and less than 50 kg by Mn-rich phases).

During the low flow, clays (except kaolinite) and Fe-rich aluminosilicate aggregates were also the main As-carriers and they contained more arsenic than during the high flow. Iron oxyhydroxides were very low As-concentrated and in addition, they were rarely present in SPM. A few particles were more As-rich like Mn-rich particles and arsenate minerals but they

were not very frequent. Hence, during this hydrological period, about 280 kg was exported by clays and Fe-rich clays and 20 kg by (Fe,Mn)oxyhydroxides.

At the particle scale, all the As-bearing phases were more As-concentrated during the low flow than the high flow except transported Fe oxyhydroxides. At a larger observation scale with bulk concentrations in SPM and in the so-called “dissolved fraction” ($< 0.45 \mu\text{m}$ operationally defined fraction, results described in Grosbois et al., 2009), As bulk concentrations mimicked these observations. In SPM, bulk As concentrations decreased with discharge, being the highest (790–1520 mg/kg) at the end of the low flow 2004 (Fig. 7) like in the most abundant As-carriers. In the “dissolved fraction”, surface waters were also more As-concentrated during the low flows 2004 and 2005 than during the high flow (Fig. 7; Grosbois et al., 2009).

Regarding potential release of arsenic from As-bearing particles towards the aqueous fraction, the partition coefficient $K_d(\text{As})$ was calculated according to Stumm and Morgan (1996), representing the ratio between As bulk concentration in SPM and in the dissolved fraction ($0.45 \mu\text{m}$ filtered). Suspended particulate matter is mineralogically very heterogeneous and thus, they contain various complexation/sorption sites, surface areas, electric charges and ligands. Partition coefficients are usually used to describe TE transfers from the solid to the aqueous compartments. However, has to be taken into account the particle concentration effect (PCE; O'Connor and Conolly, 1980) which represents the fact that K_d values usually decline with SPM concentration increase,. The PCE can be influenced by particle size, sorption kinetics, presence of various ligands, filtration artefacts with the contribution of colloids (Benoit and Rozan, 1999). In this study, the relationship between $K_d(\text{As})$ and SPM concentrations clearly shows this PCE (Fig. 7), showing very well-marked temporal variation of $K_d(\text{As})$. At the end of the low flow 2004, $K_d(\text{As})$ values were the highest (high particulate As bulk concentrations, low “dissolved” As concentrations). Arsenic showed a greater affinity to particles rather than the aqueous fraction. Origins of dissolved As in surface waters were mainly linked to “aquifer flush”, i.e. partial replacement of more or less stagnant As-rich groundwater by meteoric water (Grosbois et al., 2009). Part of dissolved As could be then sorbed on SPM.

During the high flow, $K_d(\text{As})$ values decreased. This evolution was consistent with the PCE, i.e. with a dilution by colloids and more numerous large particles in SPM, less concentrated in As due to lower surface areas. This could also be linked to changes in particle mineralogical sources, mobilized by mechanical erosion. In this study, kaolinite-type particles, being less As-concentrated ([Manning and Goldberg, 1996] and [Manning and Goldberg, 1997]), were mostly present during this high flow period.

During the next low flow period 2005, $K_d(\text{As})$ values were very low despite the fact that both “dissolved” and solid As bulk concentrations re-increased again. Arsenic bulk concentrations, increasing in SPM, were consistent with observations of higher As concentrations in particles during the low flow. However, $K_d(\text{As})$ variations were limited by the increasing of dissolved As concentrations . Dissolved As increase may be related to (i) additional sources to surface waters during this hydrological period. As temperature and dissolved sulphates concentrations also increased, sulphide alteration by microorganisms in aquifer waters have been suggested to explain the As dissolved concentrations (Grosbois et al., 2009), (ii) in the same time, As colloidal fraction could also increase, contributing to increase the so-called As “dissolved

fraction” and (iii) As could become more mobile as it may desorb more easily during this period with competition with high levels of organic matter and/or phosphates.

5. Conclusions

Trace element transfers from the solid fraction to the aquatic environment mostly depend on TE-carrier stability during the solid transport. This study focuses on the characterization of arsenic-bearing phases in SPM with observations at a particle scale. It illustrates the interest of coupling these observations at a particle scale with bulk information in SPM and dissolved fractions in order to target the fate of such a contaminant in the solid fraction. During the solid transport of SPM, arsenic was hosted in multiple phases. These different carriers had variable abundances and concentrations throughout the hydrological cycle and thus a different degree of stability along the hydrological cycle. The most common As-bearing phases here were clays and Fe-rich clay aggregates associated to Fe-oxyhydroxides, either as fine discrete grains or/and as coating on clay aggregates. The mineralogy of these As-bearing phases varied according to the different particle sources involved. They were also the least concentrated of all the identified As-bearing phases and they contained relatively more As during the low flow than during the high flow. Iron oxyhydroxides were the second most frequent type of As-carriers and had higher As levels than clay aggregates. Iron oxyhydroxides probably acted as major As-carriers in SPM during the high flow, likely involving As-rich, fresh authigenic gel-like material (ferrihydrite-type) from riverbanks, surrounding wetlands and mining sites. Their formation occurred mainly during the low flow but they were mobilized by mechanical erosion only during the high flow period when water level increased. On the other hand, the observed Mn oxyhydroxides had higher As concentrations during the low flow. Additional As-bearing phases such as arsenate minerals and Mn-rich hydrous silicates were identified but no temporal variations in mineralogy and As contents were observed due to their low abundance. The present work has shown that the relative occurrence of As-bearing phases in river SPM varied over a hydrological cycle, inducing variable As associations with the solid phases.

Acknowledgments

The financial support of this project was provided by the “Conseil Régional du Limousin”. The authors would like to thank M. Peymirat (Univ. Limoges) for thin section preparations from Teflon filters and F. Moatar (Univ. Tours) and EC2CO program (INSU/CNRS, VARIFLUX project) for funding travels to Berkeley (Ca, USA). The Advanced Light Source is supported by the Director, Office of Science, Office of Basic Energy Sciences, Materials Science Division, of the US Department of Energy under Contract No. DE-AC02-05CH11231 at Lawrence Berkeley National Laboratory. The micro-diffraction program at the ALS on beamline 12.3.2 was made possible by NSF grant # 0416243. The authors really appreciate all the detailed review of Pr Drahota and an anonymous reviewer for improving the manuscript.

References

Anawar et al., 2010 H.M. Anawar, M. Mihaljevic, A. Garcia-Sanchez, J. Akai and A. Moyano, Investigation of sequential chemical extraction of arsenic from sediments: variations in sample treatment and extractant. *Soil Sed Contam Intern J*, **19** 2 (2010), pp. 133–141.

Applin, 1958 R.N. Applin, Manganese deposits of Southwestern Oregon, *Report of investigation 5369, Bureau of mines* (1958).

Audry et al., 2006 S. Audry, G. Blanc and J. Schäfer, Solid state partitioning of trace metals in suspended particulate matter from a river system affected by smelting waste drainage. *Sci Total Environ*, **363** (2006), pp. 216–236.

Belzile et al., 1989 N. Belzile, P. Lecomte and A. Tessier, Testing readsorption of trace elements during partial chemical extractions of bottom sediments. *Environ Sci Technol*, **23** (1989), pp. 1015–1020

Benoit and Rozan, 1999 G. Benoit and T.F. Rozan, The influence of size distribution on the particle concentration effect and trace metal partitioning in rivers. *Geochim Cosmochim Acta*, **63** 1 (1999), pp. 113–127.

Bergaya et al., 2006 F. Bergaya, B.K.G. Theng and G. Lagaly, *Handbook of clay science*, Elsevier (2006) [1224 pp.].

Berrueta et al., 1995 L.A. Berrueta, B. Gallo and F. Vicente, A review of solid extraction: basic principles and new developments. *Chromatographia*, **40** 7/8 (1995), pp. 474–483.

Bodénan et al., 2004 F. Bodénan, P. Baranger, P. Piantone, A. Lassin, M. Azaroual and E. Gaucher, Arsenic behavior in gold-ore mill tailing, Massif Central, France: hydrogeochemical study and investigations of in situ redox signatures. *Appl Geochem*, **19** (2004), pp. 1785–1800.

Bossy et al., 2010 A. Bossy, C. Grosbois, S. Beauchemin, A. Courtin-Nomade, W. Hendershot and H. Bril, Alteration of As-bearing phases in a small watershed on a high grade arsenic-geochemical anomaly (French Massif Central). *Appl Geochem*, **25** (2010), pp. 1889–1901.

Bouchot et al., 1989 V. Bouchot, Y. Gros and M. Bonnemaison, Structural controls on the auriferous shear zones of the Saint Yrieix District, Massif Central, France; evidence from the Le Bourneix and Laurieras gold deposits. *Economic Geol*, **84** 5 (1989), pp. 1315–1327. |

Cancès et al., 2008 B. Cancès, F. Juillot, G. Morin, V. Laperche, D. Polya and D.J. Vaughan, *et al.* Changes in arsenic speciation through a contaminated soil profile: a XAS based study. *Sci Total Environ*, **397** (2008), pp. 178–189.

Carter et al., 2006 J. Carter, D.E. Walling, P.N. Owens and G. Leeks, Spatial and temporal variability in the concentration and speciation of metals in suspended sediment transported by the River Aire, Yorkshire, UK. *Hydrol Process*, **20** (2006), pp. 3007–3027

Chery and Gateau, 1998 L. Chery and C. Gateau, Mise à disposition de l'inventaire géochimique sur le territoire national (pour identifier les zones à risques de teneurs naturelles élevées en métaux lourds dans les eaux destinées à l'AEP) *BRGM Report R40207* (1998).

Cornell and Schwertmann, 1996 R.M. Cornell and U. Schwertmann, The iron oxides: structures, properties, reactions, occurrences and uses, (Wiley ed.) (1996), [571 pp.].

Courtin-Nomade, 2001 Courtin-Nomade, A. Mobilité de l'arsenic, liaisons arsenic-fer et spéciation de l'arsenic dans les haldes d'anciennes mines du Massif Central Français. Ph.D Thesis, Univ. Limoges. 2001..

Courtin-Nomade et al., 2010 A. Courtin-Nomade, H. Bril, J.M. Beny, M. Kunz and N. Tamura, Sulfide oxidation observed using micro-Raman spectroscopy and micro-X-ray diffraction: the importance of water/rock ratios and pH conditions. *Am Min*, **95** 4 (2010), pp. 582–591.

Croteau et al., 2005 M.N. Croteau, S.N. Luoma and A.R. Stewart, Trophic transfer of metals along freshwater food webs: evidence of Cd biomagnification in nature. *Limnol Oceanogr*, **50** 5 (2005), pp. 1511–1519.

Dawson and Macklin, 1998 E.J. Dawson and M.G. Macklin, Speciation of heavy metals in floodplain and flood sediments: a reconnaissance survey of the Aire Valley, West Yorkshire, Great Britain. *Environ Geochem Health*, **20** (1998), pp. 67–76.

Deer et al., 1967 W.A. Deer, R.A. Howie and J. Zussmann, Rock-forming minerals, *Sheet silicates*, **vol. 3** (6th ed.), (1967).

Dixit and Hering, 2003 S. Dixit and J.G. Hering, Comparison of arsenic V and arsenic III sorption onto iron oxide minerals: implications for As mobility. *Environ Sci Technol*, **37** (2003), pp. 4182–4198.

Drahota and Filippi, 2009 P. Drahota and M. Filippi, Secondary arsenic minerals in the environment: a review. *Environ Int*, **35** (2009), pp. 1243–1255.

Drahota et al., 2009 P. Drahota, J. Rohovec, M. Filippi, M. Mihaljevic, P. Rychlovsy and V. Cerveny, *et al.* Mineralogical and geochemical controls of arsenic speciation and mobility under different redox conditions in soil, sediment and water at the Mokrsko-west gold depositi, Czech Republic. *Sci Total Environ*, **407** (2009), pp. 3327–3384.

Eggleton and Guggenheim, 1986 R.A. Eggleton and S. Guggenheim, A re-examination of the structure of ganophyllite. *Min Mag*, **50** (1986), pp. 307–315

Eman et al., 2009 J.A. Eman, E. Rastade, F. Bouzari and O.N. Rashidnezhad, An introduction to individual disseminated-veinlet and vein mineralization of Cu (Pb-Zn) in the Chahmoosa-Gholekaftaran mining district, Eastern part of Toroud-Chahshirin magmatic arc. *Geosciences*, **18** (2009), pp. 112–125.

Gautier et al., 2006 J. Gautier, C. Grosbois, A. Courtin-Nomade, J.P. Floc'h and F. Martin, Transformation of natural As-associated ferrihydrite downstream a remediated mining site. *Eur J Mineral*, **18** (2006), pp. 187–195.

Gibbs, 1977 R. Gibbs, Transport phases of transition metals in Amazon and Yukon Rivers. *Geol Soc Am Bull*, **88** (1977), pp. 829–843.

Gleyzes et al., 2002 C. Gleyzes, S. Tellier and M. Astruc, Fractionation studies of trace elements in contaminated soils and sediments: a review of sequential extraction procedures. *Tends Anal Chem*, **21** 6/7 (2002), pp. 451–467.

Gordeev et al., 2004 V.V. Gordeev, V. Rachold and I.E. Vlasova, Geochemical behaviour of major and trace elements in suspended particulate material of the Irtysh river, the main tributary of the Ob river, Siberia. *Appl Geochem*, **19** (2004), pp. 593–610.

Grosbois et al., 2007 C. Grosbois, A. Courtin-Nomade, F. Martin and H. Bril, Transportation and evolution of trace element bearing phases in stream sediments in a mining — influenced basin (Upper Isle River, France). *Appl Geochem*, **11** (2007), pp. 2362–2374.

Grosbois et al., 2009 C. Grosbois, J. Schäfer, H. Bril, G. Blanc and A. Bossy, Deconvolution of trace elements (As, Cr, Mo, Th, U) sources and pathways to surface waters of a gold mining-influenced watershed. *Sci Total Environ*, **407** (2009), pp. 2063–2076.

Hochella et al., 2005 M. Hochella, J. Moore, C. Putnis, A. Putnis, T. Kasama and D. Eberl, Direct observation of heavy metal–mineral association from the Clark Fork River Superfund Complex: implications for metal transport and bioavailability. *Geochim Cosmochim Acta*, **69** 7, 1 (2005), pp. 1651–1663.

Horowitz, 1991 A.J. Horowitz, A primer on sediment-trace element chemistry (2nd ed.), Lewis Publishers (1991).

Hughes et al., 2003 J.M. Hughes, J. Rakovan, R. Bracco and M.E. Gunter, The atomic arrangement of the ganophyllite-group modulated layer silicates as determined from the orthorhombic dimorph of tamaite, with the elusive 16.8 Å ganophyllite-group superstructure revealed. *Am Min*, **88** (2003), pp. 1324–1330.

Juillot et al., 1999 F. Juillot, Ph. Ildefonse, G. Morin, G. Calas, A.M. de Kersabiec and M. Benedetti, Remobilization of arsenic from buried wastes at an industrial site: mineralogical and geochemical control. *Appl Geochem*, **14** (1999), pp. 1031–1048.

Kersten, 2002 M. Kersten, Speciation of trace elements in sediments, A.M. Ure, C.M. Davidson, Editors , *Chemical speciation in the environment* (2002) [452 pp.].

Kheboian and Bauer, 1987 C. Kheboian and C.F. Bauer, Accuracy of selective extraction procedures for metal speciation in model aquatic sediments. *Anal Chem*, **59** (1987), pp. 1417–1423.

Kierczak et al., 2009 J. Kierczak, C. Neel, J. Puziewicz and H. Bril, Mineralogy and natural weathering of slags produced by the smelting of Ni–ores (Szklary, SW Poland). *Can Min*, **47** (2009), pp. 557–572.

Kunz et al., 2009 M. Kunz, N. Tamura, K. Kai Chen, A.A. MacDowell, R.S. Celestre and M.M. Church, *et al.* A dedicated superbend x-ray microdiffraction beamline for materials, geo-, and environmental sciences at the advanced light source, . *Rev Sci Instrum*, **80** (2009) [art. no 035108].

Lin and Puls, 2000 Z. Lin and R.W. Puls, Adsorption, desorption and oxidation of arsenic affected by clay minerals and aging process. *Environ Geol*, **39** (2000), pp. 753–759. |

Manning and Goldberg, 1996 B.A. Manning and S. Goldberg, Modeling arsenate competitive adsorption on kaolinite, montmorillonite and illite. *Clays Clay Min*, **44** (1996), pp. 609–623.

Manning and Goldberg, 1997 B.A. Manning and S. Goldberg, Adsorption and stability of arsenic (III) at the clay mineral–water interface. *Environ Sci Technol*, **31** (1997), pp. 2005–2011

Masson et al., 2007 M. Masson, J. Schäfer and G. Blanc, Seasonal variations and annual fluxes of arsenic in three contrasting watersheds: the Garonne, Dordogne and Isle Rivers. *Sci Total Environ*, **373** (2007), pp. 196–207.

Nicaud, 2001 J. Nicaud, Contrôle structural de la mise en place des minéralisations aurifères du District de Saint-Yrieix-la-Perche (Massif Central français): analyse de la fracturation et étude des alterations hydrothermales. Univ. Limoges, (2001).

O'Connor and Conolly, 1980 D.J. O'Connor and J.P. Conolly, The effect of concentration and adsorbing solids on the partition coefficient. *Water Res*, **14** (1980), pp. 1517–1523.

Paquin and Di, 2003 P.R. Paquin and D.M. Di, Metals in aquatic systems: a review of exposure, bioaccumulation and toxicity modes, (Lavoisier ed.) (2003), [140 pp.].

Patkunc et al., 2004 D. Patkunc, A. Foster, S. Heald and G. Laflamme, Speciation and characterization of arsenic in gold ores and cyanidation tailings using X-ray absorption spectroscopy. *Geochim Cosmochim Acta*, **68** 5 (2004), pp. 969–983.

Peacor et al., 1984 D.R. Peacor, P.J. Dunn and W.B. Simmons, Eggletonite, the Na analogue of ganophyllite. *Min Mag*, **48** (1984), pp. 93–96

Pedersen et al., 2006 H.D. Pedersen, D. Postma and R. Jakobsen, Release of arsenic associated with the reduction and transformation of iron oxides. *Geochim Cosmochim Acta*, **70** (2006), pp. 4116–4129.

Piantone et al., 1994 P. Piantone, X. Wu and J.C. Touray, Zoned hydrothermal alteration and genesis of the gold deposit at Le Chatelet (French Massif Central). *Economic Geol*, **89** 4 (1994), pp. 757–777.

Proust et al., 1986 D. Proust, J.P. Eymery and D. Beaufort, Supergene vermiculitization of a magnesian chlorite: iron and magnesium removal processes. *Clays Clay Min*, **34** 5 (1986), pp. 572–580.

Robin and Molina, 2006 E. Robin and E. Molina, Chronostratigraphy, composition, and origin of Ni-rich spinel from the Late Eocene Fuente Caldera section in Spain: one impact or more. *Meteor Planet Sci*, **41** 8 (2006), pp. 1231–1248

Robin et al., 2003 E. Robin, C. Rabouille, G. Martinez, I. Lefevre, J.L. Reyss and P. van Beek, *et al.* Direct barite determination using SEM/EDS-ACC system: implications for constraining barium carriers and barite preservation in marine sediments. *Mar Chem*, **82** (2003), pp. 289–306.

Roussel et al., 1998 C. Roussel, H. Bril and A. Fernandez, Hydrogeochemical survey and mobility of As and heavymetals on the site of a former gold mine (saint Yrieix mining district, France). *Hydrogéologie*, **1** (1998), pp. 3–12.

Roussel et al., 2000 C. Roussel, H. Bril and A. Fernandez, Arsenic speciation: involvement of environmental impact caused by mine wastes. *J Environ Qual*, **29** (2000), pp. 182–188. |

Shayan, 1984 A. Shayan, Hisingerite material from a basalt quarry near Geelonk, Victoria, Australia. *Clays Clay Minerals*, **32** 4 (1984), pp. 272–278.

Stumm and Morgan, 1996 W. Stumm and J.J. Morgan, Aquatic chemistry, (third ed.), Wiley, New York (1996).

Tamura et al., 2005 N. Tamura, H.A. Padmore and J.R. Patel, High spatial resolution stress measurements using synchrotron based scanning X-ray microdiffraction with white or monochromatic beam. *Mater Sci Eng A*, **399** (2005), pp. 92–98.

Tessier et al., 1979 A. Tessier, P. Campbell and M. Bisson, Sequential extraction procedure for the speciation of particulate trace metals. *Anal Chem*, **1** 7 (1979), pp. 844–851

Tipping et al., 1979 E. Tipping, V.K. Hetherington and P.M. Clayton, Specific and non specific sorption of cadmium by soil clays as influenced by zinc and calcium. *Aust J Soil Res*, **17** (1979), pp. 17–28.

Touray et al., 1989 J.C. Touray, E. Marcoux, P. Hubert and D. Proust. *Economic Geol*, **84** 5 (1989), pp. 1328–1339. |

Velde, 1985 B. Velde, Clay minerals: a physico-chemical explanation of their occurrence, Elsevier, Amsterdam (1985) [427 pp.].

Wang and Fisher, 2009 W. Wang and N.S. Fisher, Assimilation efficiencies of chemical contaminants in aquatic invertebrates: a synthesis. *Environ Toxicol Chem*, **18** 9 (2009), pp. 2034–2045.

Zhu et al., 2006 Y.N. Zhu, X.H. Zhang, Q.L. Xie, D.Q. Wang and G.W. Cheng, Solubility and stability of calcium arsenates at 25 °C. *Water Air Soil Pollut*, **169** (2006), pp. 221–238.

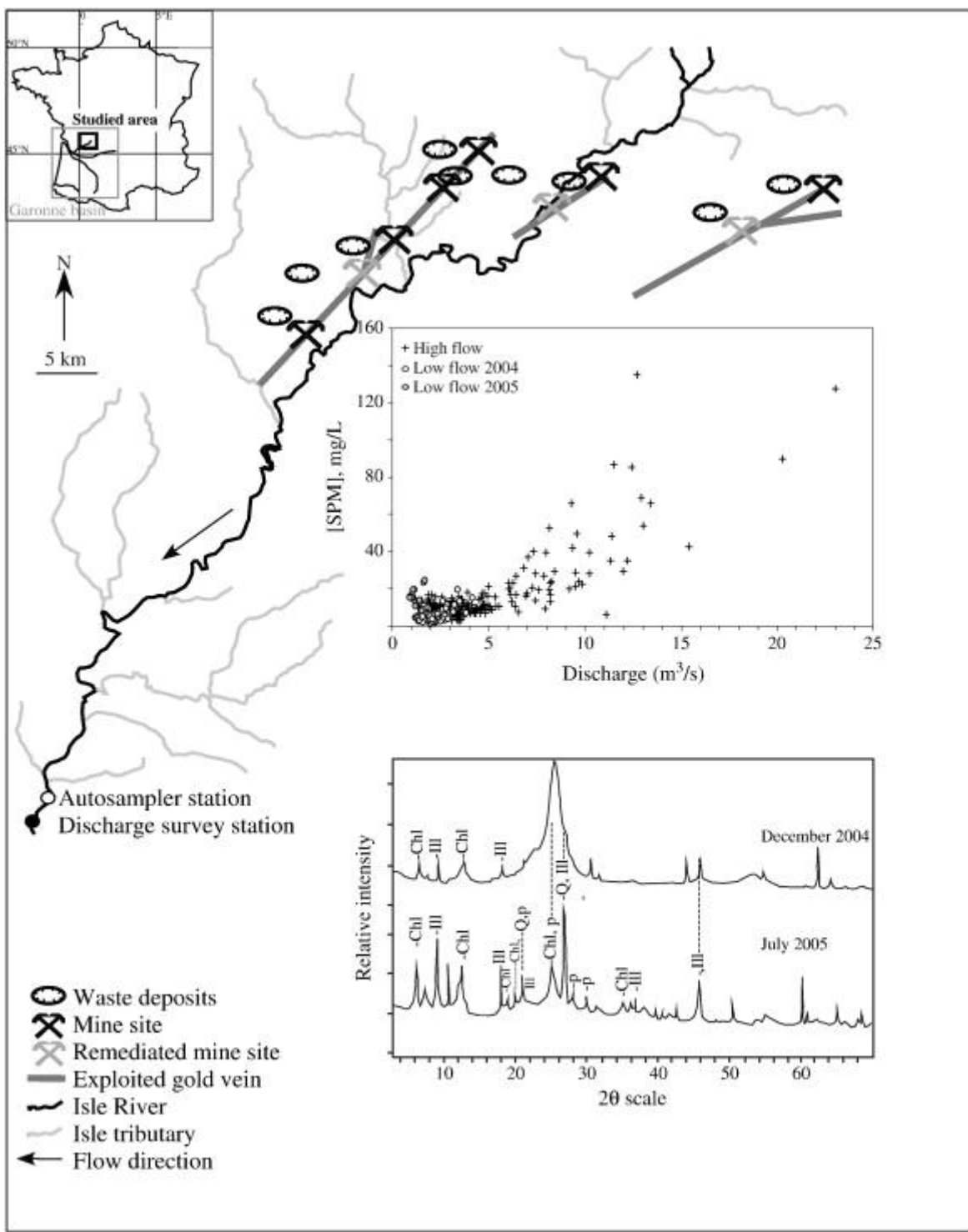


Fig. 1. : Localization of discharge and autosampler monitoring stations in the Isle River Upper Basin. Also shown variations of daily discharge (m^3/s) and daily suspended matter concentrations ([SPM], mg/L) plus representative X-ray diffraction (Cu-K α) spectra of suspended material collected in December 2004 (high flow period) and in July 2005 (low flow period). (Chl = chlorite, Ill = illite, Q = quartz, p = plagioclases).

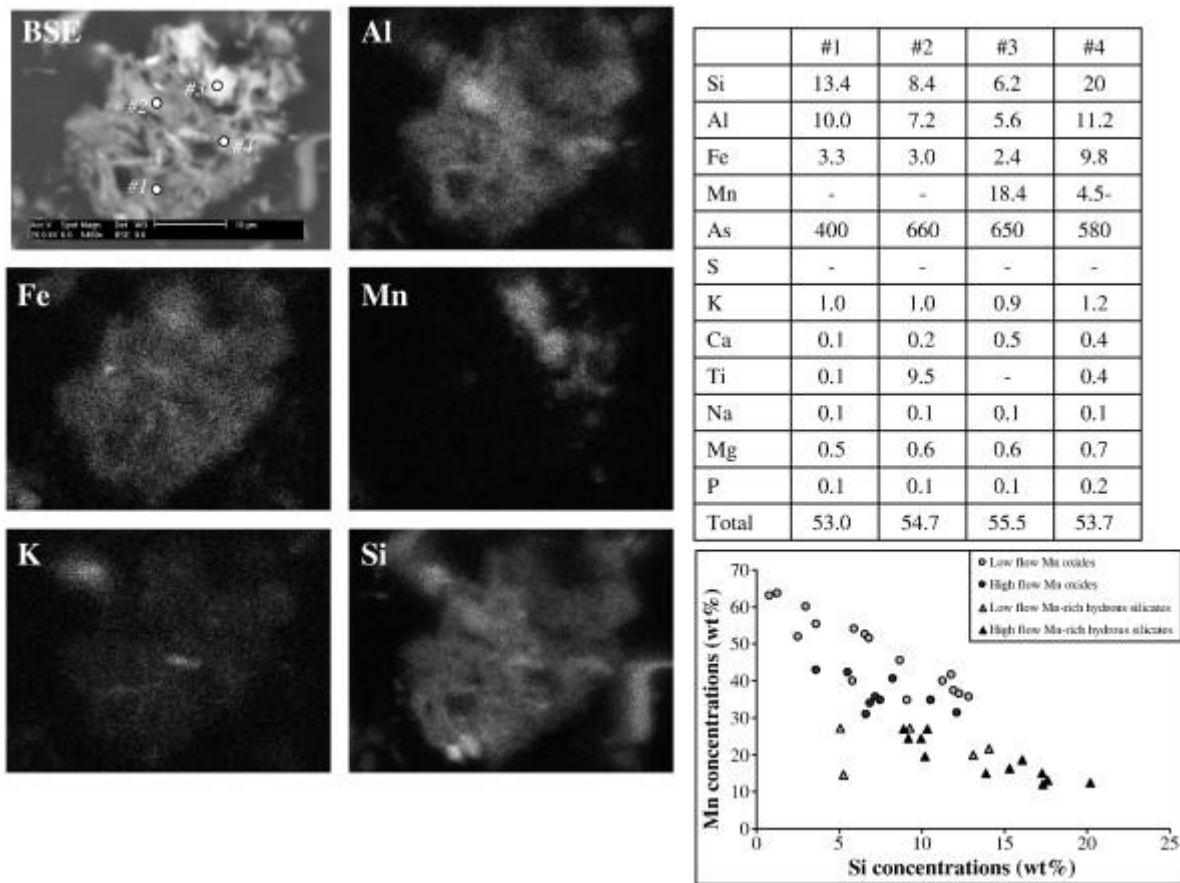


Fig. 2. : BSE microscope image of a representative clay aggregate with associated EPMA analyses and SEM-X ray elemental maps and the relationship between Si and Mn concentrations, as determined by EPMA, in Mn-oxyhydroxides and Mn-rich hydrous silicates for both the high and the low flow periods. All concentrations are in wt% except As in mg/kg and total in %.

Table 1. Range of chemical composition (wt%) of As-bearing phases transported in suspended particulate matter during the high flow (a) and the low flow (b). n = number of analyzed particles with both EPMA and SEM/EDS-ACC techniques, (n) represents the number of analyzed particles with only SEM/EDS-ACC technique used for representative occurrence calculation. d.l. = below detection limit. *Concentrations were acquired with only SEM/EDS-ACC technique. Norm = normalized concentration (see text for calculations).

(a) High flow	Si norm	Al norm	Fe norm	Mn norm	Mg norm	Ca norm	Na* norm	K norm	Ti norm	P norm	S* norm	As norm	Total
Clays; n = 255 (255) representing 57% of As-bearing phases during this period													
Min	17.7	10.7	0.3	d.l.	d.l.	d.l.	d.l.	d.l.	d.l.	d.l.	d.l.	0.10	46.6
Max	45.1	29.6	10.5	2.5	6.1	7.2	11.3	10.5	11.6	2.9	2.3	1.58	54.6
Fe-rich Clays; n = 142 (142) representing 32% of As-bearing phases during this period													
Min	12.4	7.9	8.1	d.l.	0.7	0.2	d.l.	0.3	d.l.	d.l.	0.1	0.11	53.1
Max	30.9	16.4	25.3	7.4	11.5	8.6	8.4	4.4	7.2	5.9	3.5	1.43	59.5
Fe oxyhydroxydes; n = 31 (31) representing 7% of As-bearing phases during this period													
Min	2.9	2.4	26.7	d.l.	d.l.	0.1	d.l.	d.l.	d.l.	d.l.	0.2	0.12	55.0
Max	15.3	12.0	55.7	4.9	2.9	8.5	12.3	0.8	0.3	3.1	3.0	2.48	64.9
Mn oxyhydroxydes; n = 9 (9) representing < 2% of As-bearing phases during this period													
Min	3.6	2.5	2.2	30.8	0.9	0.4	d.l.	d.l.	d.l.	d.l.	0.5	0.16	57.3
Max	12.1	8.6	12.9	42.8	2.7	3.4	8.1	1.1	d.l.	0.7	2.3	0.79	68.2
Mn-rich silicates*; n = 12 (12) representing < 3% of As-bearing phases during this period													
Min	8.9	4.7	4.2	12.0	0.4	0.5	d.l.	d.l.	d.l.	d.l.	0.2	0.17	55.4
Max	20.2	12.8	15.1	26.9	2.5	5.1	4.5	2.2	0.3	0.5	1.3	0.71	64.7
(b) Low flow	Si norm	Al norm	Fe norm	Mn norm	Mg norm	Ca norm	Na* norm	K norm	Ti norm	P norm	S* norm	As norm	Total
Clays; n = 142 (110) representing 75% of As-bearing phases during this period													
Min	15.9	10.5	0.2	d.l.	d.l.	d.l.	d.l.	d.l.	d.l.	d.l.	d.l.	0.10	41.2
Max	45.3	26.4	14.7	24.5	7.7	19.7	12.3	8.6	19.1	1.5	3.7	1.55	71.7
Fe-rich Clays; n = 52 (26) representing 18% of As-bearing phases during this period													
Min	10.8	7.9	10.8	d.l.	0.1	d.l.	d.l.	d.l.	d.l.	d.l.	d.l.	0.11	41.8
Max	28.8	20.5	35.5	18.2	10.3	3.6	6.1	2.8	6.4	2.8	2.0	1.42	72.9
Fe oxyhydroxydes; n = 48 (3) representing < 3% of As-bearing phases during this period													
Min	0.3	d.l.	34.8	d.l.	d.l.	0.3	d.l.	d.l.	d.l.	d.l.	d.l.	0.10	51.7
Max	15.1	16.1	76.4	3.9	5.9	3.4	4.6	2.5	5.3	2.6	2.5	2.80	84.2
Mn oxyhydroxydes; n = 20 (4) representing < 3% of As-bearing phases during this period													
Min	0.8	0.6	2.8	34.6	0.3	0.9	d.l.	0.1	d.l.	d.l.	d.l.	0.14	40.4
Max	12.9	11.1	23.6	63.6	1.6	5.9	1.1	2.0	1.2	1.9	0.7	1.26	57.8
Mn-rich silicates*; n = 4 (4)													
Min	5.1	7.4	5.3	20.0	1.1	0.2	1.7	0.1	d.l.	0.2	0.6	0.11	60.5

(a) High flow	Si	Al	Fe	Mn	Mg	Ca	Na*	K	Ti	P	S*	As	Total
Max	14.1	12.2	19.2	27.2	1.6	1.1	5.8	0.8	0.2	0.6	1.6	0.61	66.2
Arsenate type*; n = 7 (7)													
min	d.l.	3.3	0.6	d.l.	d.l.	d.l.	d.l.	d.l.	d.l.	d.l.	4.6	14.56	54.2
max	15.2	6.0	3.0	0.3	0.8	16.8	5.1	0.2	0.1	d.l.	11.7	41.36	59.3

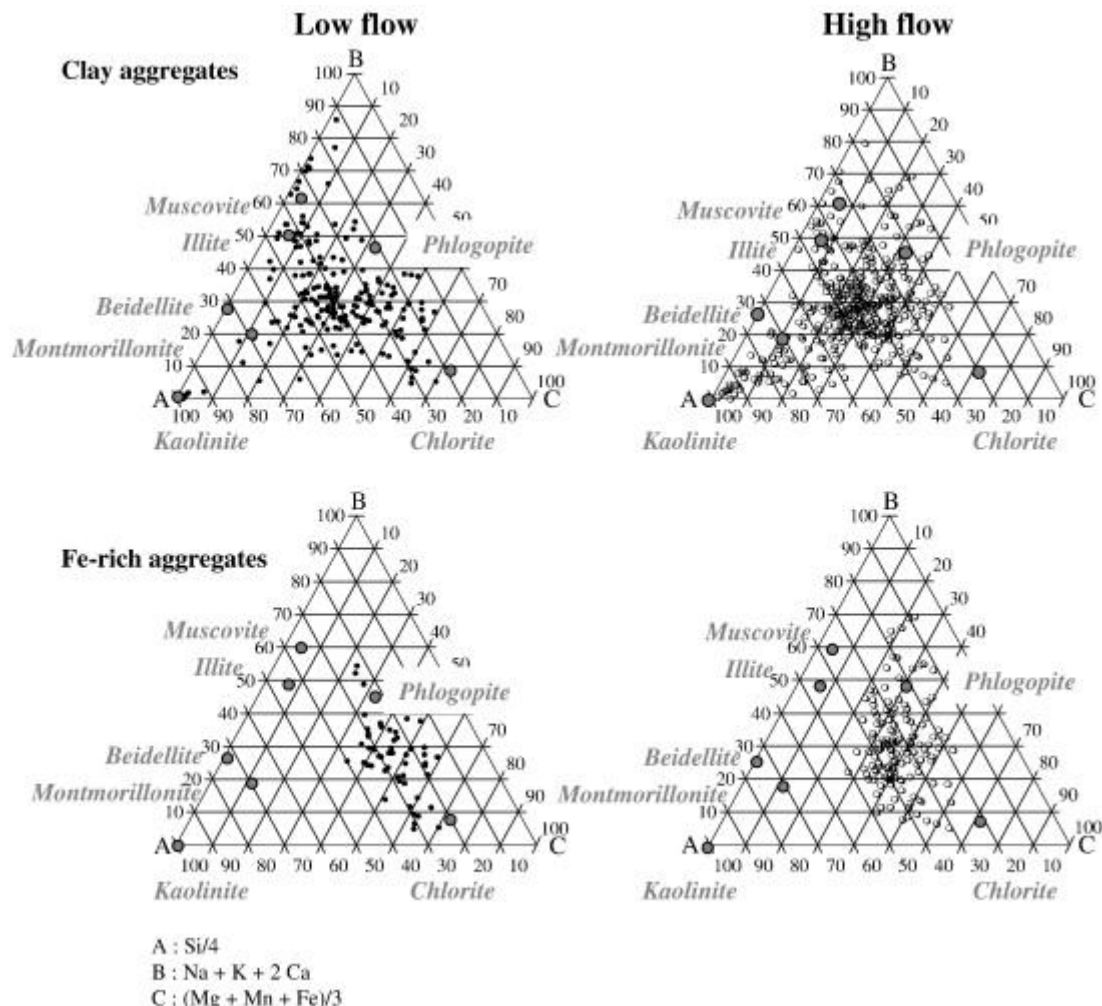


Fig. 3. : Classification of clays and Fe-rich clays according to Velde (1985), based on chemical analyzes at a particle scale during the low flow (closed circles) and the high flow (open circles). Chemical composition of muscovite, illite, beidellite, montmorillonite, phlogopite and chlorite are from Deer et al. (1967).

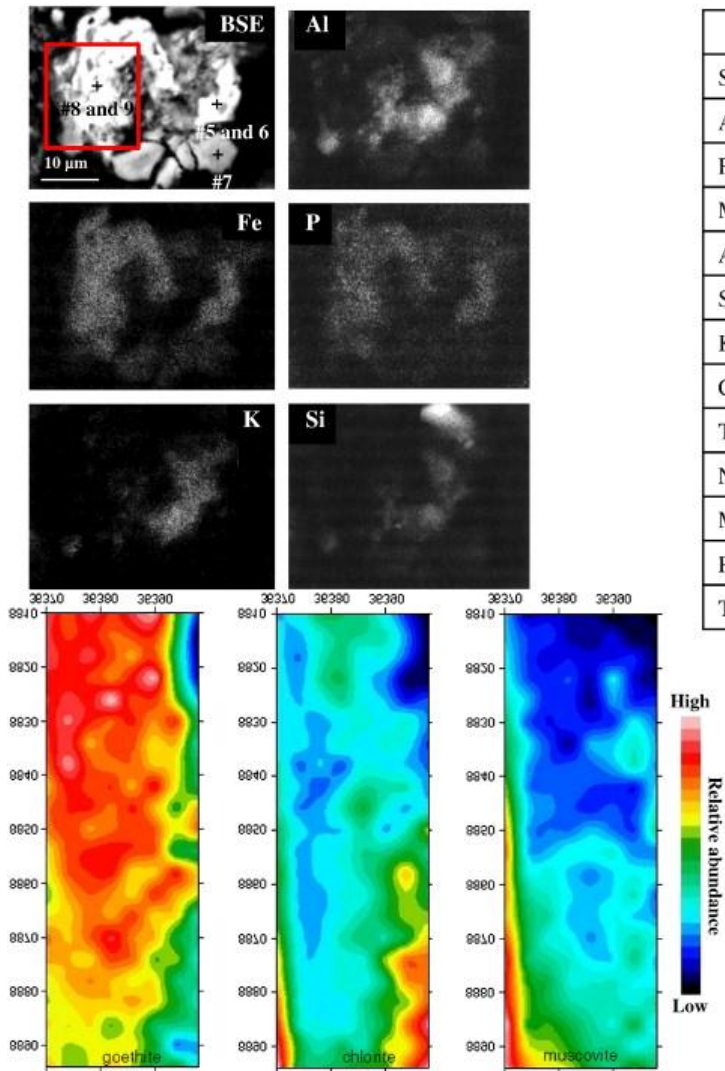


Fig. 4. : BSE microscope image of a representative grain of Fe oxyhydroxide associated to SEM-X ray elemental maps, EPMA analyses and μ XRD maps corresponding to the square in the particle and representing the distribution of goethite (4.18 Å), chlorite (7.07 Å) and muscovite (9.9 Å) respectively, their main intensity XRD peak. All concentrations are in wt.% except As in mg/kg and total in %.

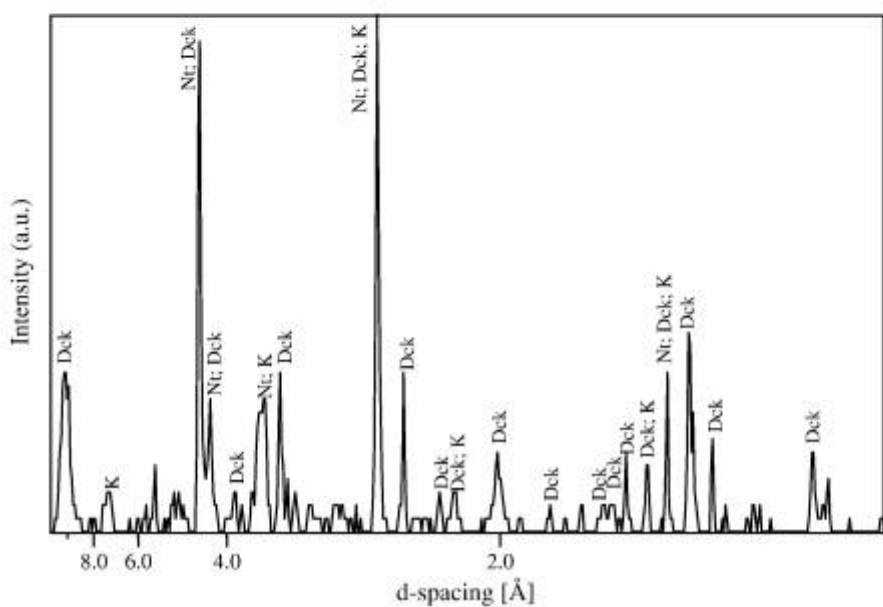
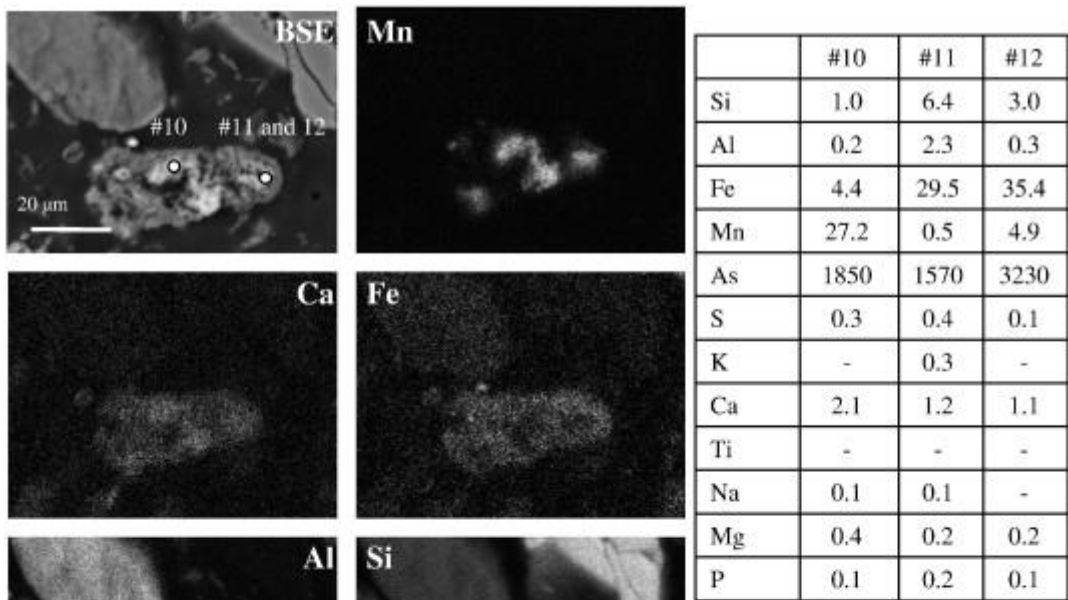


Fig. 5. : BSE microscope image of a representative grain of Fe-oxyhydroxide associated to EPMA analyses, SEM-X ray elemental maps and 2D integrated μ XRD pattern at point #10 showing the presence of kellyite (K) and neotocite (N), 2 Mn hydrous silicate, plus dickite (Dck). All concentrations are in wt.% except As in mg/kg and total in %.

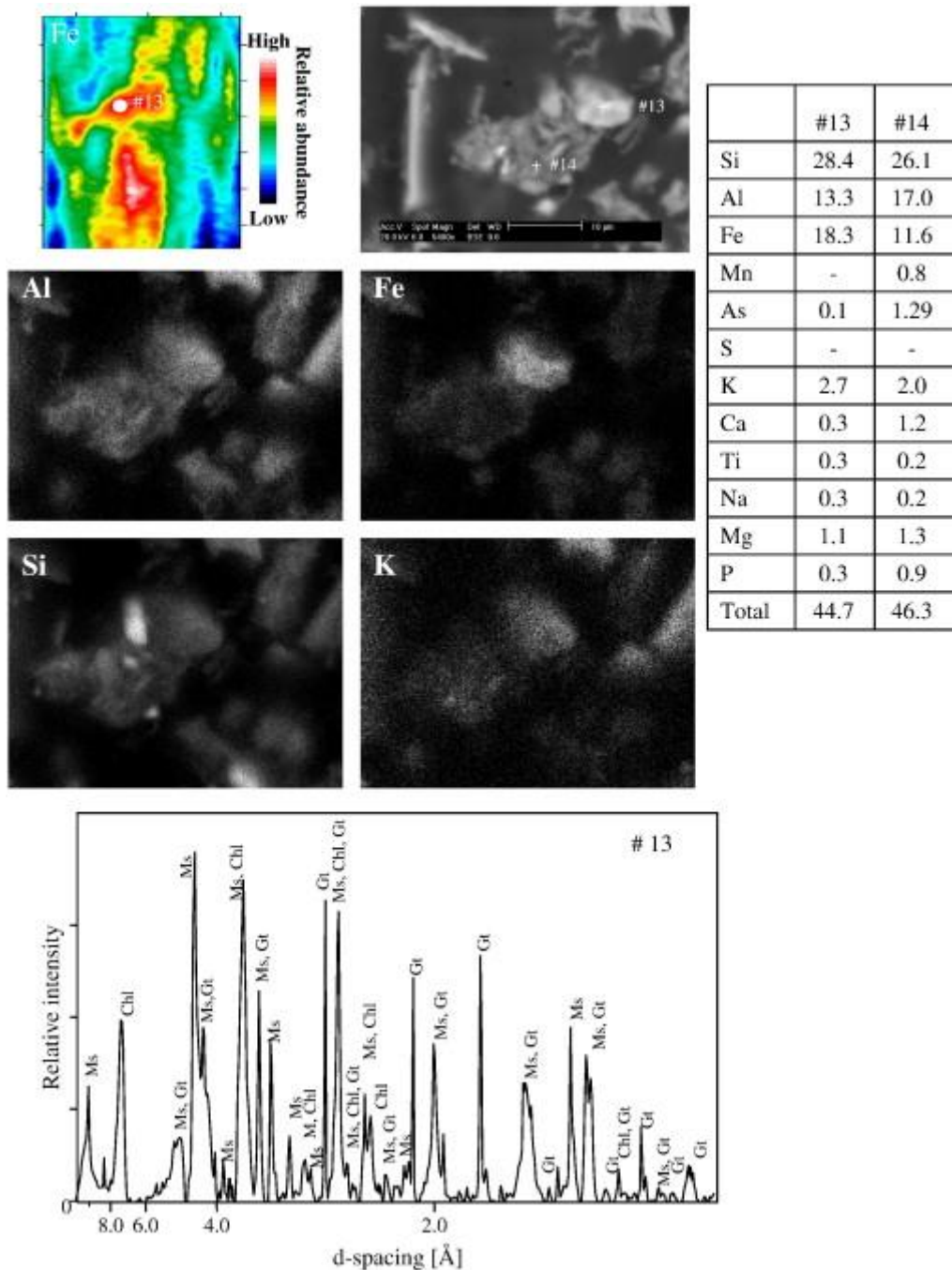


Fig. 6. : BSE microscope image of representative Fe-rich clay aggregate with associated EPMA analyses, SEM-X ray elemental maps, Fe distribution obtained by μ SXRF and integrated diffractogram obtained by μ XRD at point #13 (Ms = muscovite, Chl = chlorite, Gt = goethite). All concentrations are in wt.% except As in mg/kg and total in %.

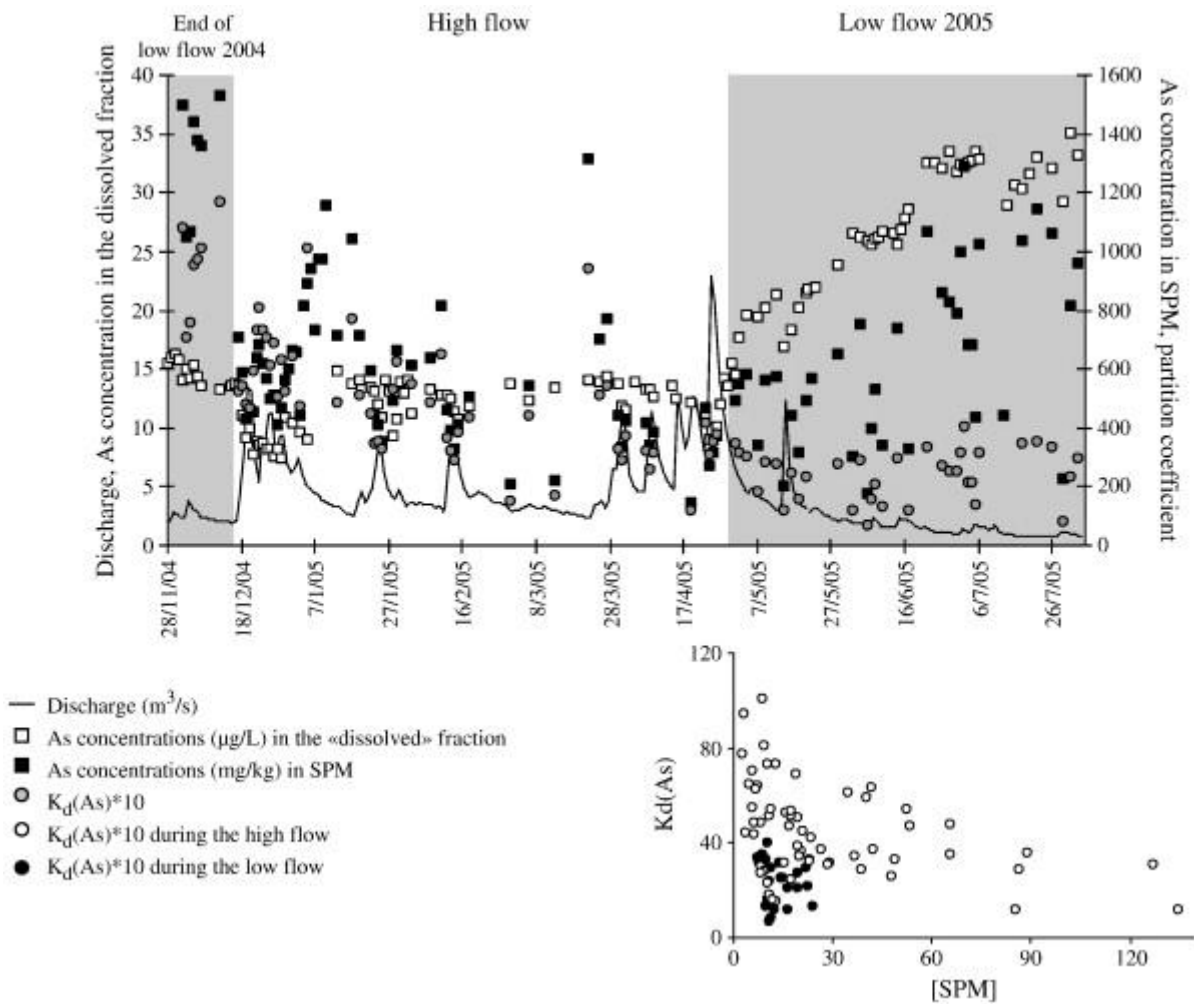


Fig. 7. : Temporal variations of discharge, bulk As in SPM (mg/kg), dissolved As ($\mu\text{g/L}$) in the associated surface waters (Grosbois et al., 2009) and the partition coefficient K_d for arsenic.